Hierarchical Carbon Nanotube Membrane-Supported Gold Nanoparticles for Rapid Catalytic Reduction of p-Nitrophenol

Haitao Wang, Zhuxin Dong, and Chongzheng Na*

Department of Civil and Environmental Engineering and Earth Sciences, University of Notre Dame, 156 Fitzpatrick Hall, Notre Dame, Indiana 46556, United States

S *Supporting Information*

ABSTRACT: Gold nanoparticles (AuNPs) have attracted increasing attention as catalysts for pollutant degradation because of their unique reactivity. Direct use of gold nanoparticles in water treatment faces prohibitive challenges from nanoparticle aggregation and post-treatment separation. To prevent nanoparticles from aggregating and eliminate the need for separation, we affixed AuNPs on hierarchical carbon nanotube membrane (HCNM) that was approximately 50 μm thin with 10 μm × 10 μm openings as pores for water passage. HCNM was fabricated by growing vertically aligned carbon nanotube (CNT) arrays on stainless steel mesh. Using p-nitrophenol (PNP) as model pollutant, we showed that in batch experiments HCNM-supported AuNPs retained 78% of their catalytic capability compared to suspended AuNPs. The slight reduction in reactivity was attributed to the blockage of part of the gold surface at the AuNP−CNT juncture. When the membrane was used in continuous flow-through operation, HCNM-supported AuNPs achieved 71% of the maximum catalytic ability measured in batch. The rapid kinetics obtained with HCNM-supported AuNPs was in great contrast to the slow kinetics that one would expect for a rigid membrane of similar configuration. For a rigid membrane, water passing through microscopic pores was confined as laminar flow and thus would not mix well with catalysts affixed on pore walls. For HCNM, CNTs aligning pore walls were flexible so that they could move vigorously to create a chaotic mixing condition and promote AuNP-catalyzed PNP reduction.

KEYWORDS: *Vertically aligned carbon nanotubes, Noble metal catalyst, Coinage metal catalyst, Industrial wastewater treatment, Heterogeneous catalysis, Monolithic support, High flux membrane*
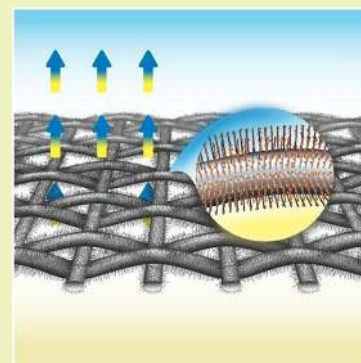
INTRODUCTION

Metal nanoparticles such as gold, silver, and iron have attracted increasing attention as catalysts and reagents for water treatment because of their unique reactivity with pathogens, pesticides, and mercury.[1] Using metal nanoparticles instead of their bulk counterparts can reduce the consumption of limited natural resources while improving treatment performance. Direct use of metal nanoparticles in water treatment, however, faces prohibitive challenges. First, metal nanoparticles tend to aggregate in water due to surface hydrophobicity. Once nanoparticles aggregate, they can lose most of reactivity as a result of reduced access to the buried surface. Second, if nanoparticles survive aggregation by adsorbing surfactant molecules such as certain types of natural organic matter,[2] the separation of metal nanoparticles after treatment can become tedious and costly. Surfactant-coated nanoparticles do not settle well under gravity and often require energy-intensive processes such as centrifugation for separation. Unsettled nanoparticles are of great concern for their potential adverse effects to humans and ecosystems.[3] Third, metal nanoparticles released with treated water must be replenished for continuous operation, which increases treatment cost. For these reasons, the use of nanoparticles, including metal nanoparticles, in water treatment is so far limited.

The double-sided dilemma of aggregation and separation associated with metal nanoparticles can be resolved by attaching them on engineering supports so that they are fixed in place against both rapid agglomeration and perpetual suspension. Engineering materials that have been proposed to support nanoparticles can be categorized into two groups. The first group includes organic and inorganic colloidal particles. Examples include polymethylmethacrylate spheres,[4] polypyrrole nanotubes,[5] polyaniline fibers,[6] ceria nanotubes,[7] silica spheres,[8] and spheres with magnetic cores.[9−13] The second group of supports consists of monolithic materials such as polymeric hollow fiber membranes[14,15] and anodic aluminum oxide (AAO) membranes.[16] The main advantage of monolithic supports is that they can be used to build flow-through units for continuous operation. In comparison, colloidal particles decorated with reactive nanoparticles are more suitable for use in batch reactors, which have to be operated intermittently. To design a suitable monolithic support, an important
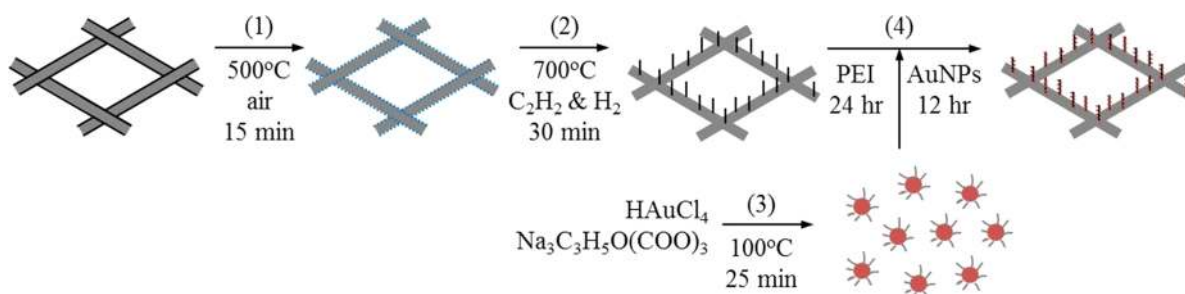
Scheme 1. Preparation of Hierarchical Carbon Nanotube Membrane-Supported Gold Nanoparticles (AuNPs). PEI: Polyethyleneimine

challenge is to create microscopic pores that can maximize both nanoparticle loading and water flux. For membranes made of rigid pores, high particle loading requires a large surface area and thus small pores, whereas high water flux requires low friction and thus large pores. The contradictory requirements create another double-sided dilemma that is seemingly impossible to overcome.

The loading-and-flux dilemma can be resolved by using monolithic supports that have hierarchical structures.[17] An example is the hierarchical carbon nanotube membrane (HCNM) that we report herein. Our HCNM was fabricated by growing vertically aligned carbon nanotube (CNT) arrays on stainless steel mesh (SSM). In HCNM, individual CNTs provide the large surface area required for high nanoparticle loading. The high water flux is achieved by using SSM with micrometer-sized openings for flow passage. Because the two tasks are fulfilled by different substructures in HCNM at different dimensional scales, they have minimal interference with each other's functions and thus can be designed independently. In this paper, we demonstrate the feasibility of HCNM for supporting gold nanoparticles (AuNPs) in the catalytic reduction of p-nitrophenol (PNP), a Clean Water Act priority pollutant,[18] in a flow-through reactor. Although HCNM has been previously proposed as catalyst support,[19,20] to our knowledge, the use of AuNPs-decorated HCNM in flow-through operation has not been documented in the literature.

■ MATERIALS AND METHODS

The fabrication of HCNM-supported AuNPs involved several steps, as illustrated in Scheme 1, including (1) activation of stainless steel mesh, (2) growth of carbon nanotube arrays, (3) synthesis of gold nanoparticles, and (4) attaching AuNPs on HCNM. The materials, reagents, equipment, and synthesis conditions used in each step, together with those used in material cauterization and evaluation, are detailed as follows.

Activation of Stainless Steel Mesh. Sheets of 304 stainless steel with a mesh size of 400×400 openings per square inch were purchased from Grainger (Lake Forest, IL) and verified by X-ray diffraction (Bruker D8 Discover; Figure S1, Supporting Information). The mesh consisted of 70% Fe, 19% Cr, and 11% Ni. To prepare for surface activation, the mesh was first cleaned by sonication in acetone for 15 min. After blowing dry using pure nitrogen, the cleaned mesh was rolled and inserted into the quartz tubing housed in a horizontal furnace (Figure S2, Supporting Information). The chamber was heated to 500 °C and held for 15 min to break the chromium-oxide passivation coating on the mesh and generate iron/nickel catalytic nanoparticles.

Growth of Carbon Nanotube Arrays. CNTs were grown using chemical vapor deposition (CVD).[22,23] Without removing the mesh from the quartz tubing after activation, temperature was ramped to 700 °C in 5 min under the flow of 300 sccm argon. Once temperature was stabilized, 20 sccm acetylene (C_2H_2) and 150 sccm hydrogen (H_2)

were introduced into the quartz tubing to initiate the growth process. After 30 min of growth, the furnace was cooled to room temperature under the protection of argon before HCNM was removed from the furnace for attaching AuNPs.

Synthesis of Gold Nanoparticles. AuNPs capped with negatively charged citrate were prepared using the Ferns method.[24] Briefly, 100 mL of 10 mg L^{-1} aurichloric acid ($HAuCl_4$, Sigma Aldrich) aqueous solution was heated to a rolling boil with vigorous stirring in a 250 mL flask. Then, 3 mL of 1 wt % trisodium citrate ($Na_3C_3H_5O(COO)_3$, Sigma Aldrich) was added rapidly to the solution. The mixture was heated with stirring for 10 min and stirred without heating for additional 15 min. The color of the solution changed from yellow to bluish gray and further to soft pink, indicating the formation of AuNPs.

Attaching AuNPs on HCNM. AuNPs were attached on the CNTs of HCNM using a layer-by-layer (LBL) assembly method. HCNM was first immersed in 2 wt % polyethyleneimine (PEI, Sigma Aldrich; molecular weight: 25000 Da) aqueous solution placed on a shaker table for 24 h. The adsorption of PEI added positive charge to the CNTs' surfaces. HCNM was rinsed with copious water to remove loose PEI molecules and then immersed in the AuNP suspension for 12 h to attach negatively charged AuNPs via electrostatic attraction (adsorption efficiency: ca. 100%).

Material Characterization. HCNM, AuNPs, and AuNPs-decorated HCNM were characterized using a series of analytical techniques. The morphologies of CNTs and AuNPs were examined using transmission and scanning electron microscopies (TEM, FEI Titan 80-300; SEM FEI Magellan 400). The crystallinity and long-range ordering of CNTs were analyzed using Raman spectroscopy (Renishaw 1000).[25] To verify the sizes of AuNPs, the absorption of visible light by the AuNP suspension was measured using UV−vis spectrophotometry (Agilent Cary 300). The successful fixation of AuNPs on HCNM was confirmed using energy-dispersive X-ray spectroscopy (EDX, Quantax 200).

Reduction of p-nitrophenol. The catalytic reduction of PNP by sodium borohydride ($NaBH_4$) was conducted using both suspended AuNPs and HCNM-supported AuNPs at ambient temperature (ca. 22 °C). For suspended AuNPs, reduction was performed in a scintillation vial used as a batch reactor. The reaction solution was prepared by mixing 0.15 mL of 4 mM PNP, 1.5 mL of 100 mM $NaBH_4$, and 1.2 mL deionized (DI) water. The concentration of PNP and $NaBH_4$ was 0.2 mM and 50 mM, respectively. PNP and $NaBH_4$ were purchased from Sigma Aldrich. DI water was generated on site using a Millipore system. To minimize decomposition of $NaBH_4$, the reduction reaction was performed within minutes after the solution was prepared. To start the reaction, 0.15 mL of 0.25 mM AuNPs was added to the reaction solution. The decrease of PNP concentration and the formation of reduction product were monitored using UV−vis spectrophotometry. The absorbance of AuNPs was subtracted from measurements using an aqueous suspension containing the same concentration of AnNPs but no PNP or $NaBH_4$.

For HCNM-supported AuNPs, reduction was performed using both batch and flow-through setups. The batch experiments were performed similar to those for AuNPs except that a piece of 0.5 cm $\times$ 0.5 cm AuNPs-decorated HCNM was used. The initial
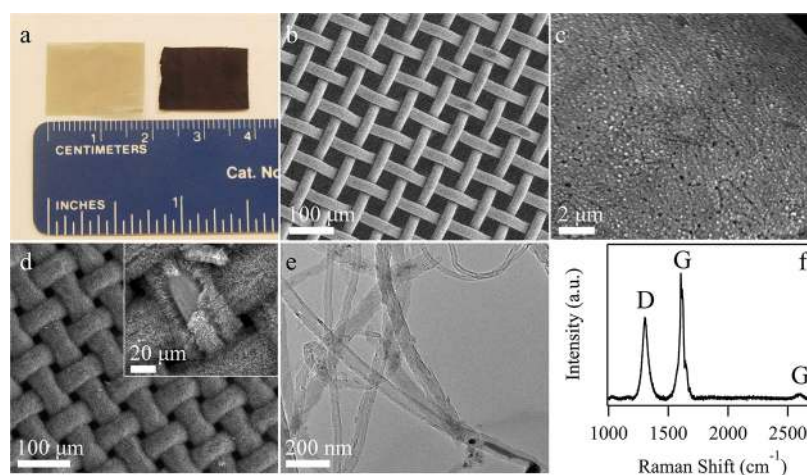
Figure 1. Hierarchical carbon nanotube membrane (HCNM). (a) Digital photos of pristine and carbon nanotube coated stainless steel meshes (SSM). (b) Scanning electron micrograph (SEM) of pristine SSM. (c) SEM of activated SSM. (d) SEM of HCNM (inset: intentionally scratched to show CNTs' vertical alignment). (e) Transmission electron micrograph of individual CNTs removed from HCNM by sonication. (f) Raman spectrum of HCNM.
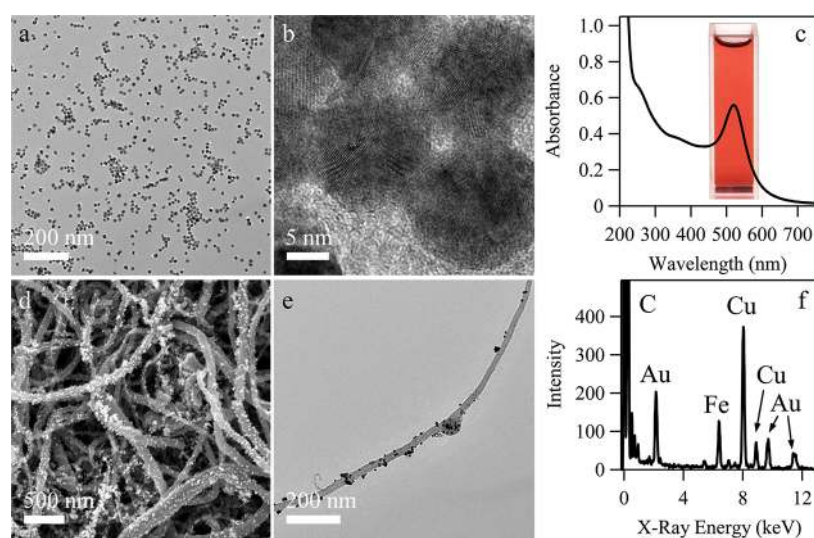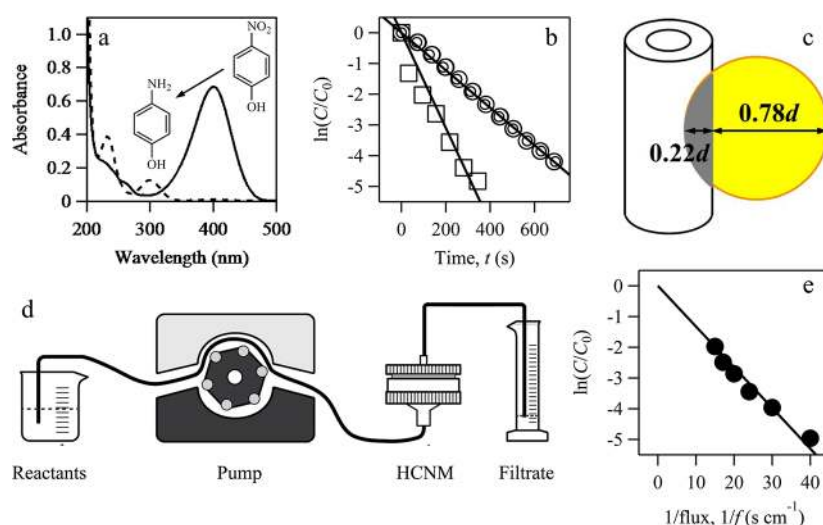

Figure 2. Gold nanoparticles (AuNPs) suspended in water and supported by hierarchical carbon nanotube membrane (HCNM). (a,b) Transmission electron micrographs (TEM) of suspended AuNPs. (c) UV−vis spectrum and digital photograph of aqueous suspension of AuNPs (50 mg L^{-1}). (d) Scanning electron micrograph of HCNM-supported AuNPs. (e) TEM of AuNP-decorated CNT removed from HCNM by sonication. (f) Energy dispersive X-ray spectrum of AuNPs-decorated HCNM.

concentration of PNP was varied among 0.05, 0.1, and 0.2 mM to rule out the dependence of reaction kinetics on initial concentration. The amount of borohydride was fixed in excess at 50 mM in all experiments. In flow-through experiments, the PNP−NaBH$_4$ solution was pumped through a piece of 1 cm^2 HCNM catalyst using a peristaltic pump. Flow rates up to 4 mL min^{-1} were used to achieve water fluxes up to 4 mL cm^{-2} min^{-1}. The reduction of PNP was quantified by periodically collecting the filtrate and measuring its light absorption.

■ RESULTS AND DISCUSSION

Hierarchical Carbon Nanotube Membrane. The physical characteristics of HCNM are summarized in Figure 1. The pristine stainless steel mesh had a metallic color before CNT growth that turned to black after growth (Figure 1a). Scanning electron microscopy revealed that SSM was woven with metal wires having a diameter of 25 μm, which formed openings of 38 μm × 38 μm (Figure 1b). The wire surface of pristine SSM was microscopically smooth; however, activating SSM in air at 500

°C created nanoparticles of 20−25 nm in size (Figure 1c). EDX showed that the nanoparticles consisted of both iron (80%) and nickel (20%), which were effective catalysts for growing arrays of multiwalled CNTs (Figure 1d).[26,27] The growth of CNTs increased the wire diameter to ca. 50 μm and reduced the openings to 10 μm × 10 μm. To examine the organization of CNT arrays, we scratched HCNM with tweezers and created an area with part of the CNT arrays removed and the underlying wire exposed. SEM with high magnification confirmed the vertical alignment of CNTs (inset of Figure 1d). To examine the quality of individual CNTs, we broke them off HCNM by sonication and transferred them onto copper grids with the aid of ethanol. Transmission electron microscopy showed that individual CNTs were hollow tubes with crystalline walls made of graphene sheets (Figure 1e). Raman spectroscopy showed an asymmetric G band associated with the diameter distribution of individual CNTs as well as a G-to-D ratio greater than unity

Figure 3. Reduction of *p*-nitrophenol (PNP) by sodium borohydride (NaBH$_4$) under the catalysis of suspended and HCNM-supported gold nanoparticles (AuNPs). (a) UV−vis absorption spectra of a reactive solution (0.2 mM PNP and 50 mM NaBH$_4$) before and after the addition of suspended AuNPs (reaction time: 15 min). (b) Decrease of normalized residual PNP concentration with reaction time in batch reactors (squares, HCNM-supported AuNPs; circles, suspended AuNPs. Circle size from large to small: 0.2, 0.1, and 0.05 mM initial PNP). (c) Blockage of part of AuNP surface at the AuNP−CNT juncture. (d) Flow-through setup for evaluating the catalytic performance of hierarchical carbon nanotube membrane (HCNM-supported gold nanoparticles. (e) Decrease of normalized residual PNP concentration with the increase of the inverse of water flux in flow-through operation using HCNM-supported AuNPs.

indicating the presence of minimal structural defects (Figure 1f).[25]

HCNM fabricated by us has significant structural improvements compared to similar materials reported recently by other researchers.[21,28−33] Previous attempts of growing CNT arrays on stainless steel mesh mostly used ethane, ethylene, benzene, or carbon monoxide as the carbon source and resulted in poor CNT quality and organization. Using acetylene as the carbon source, we have improved the self-assembly of carbon atoms in CVD, which lead to the growth of well-aligned CNTs forming a uniform forest. Most previous attempts also required etching the mesh with concentrated hydrochloride acid for CNT growth. We have eliminated the need of acid etching in our synthesis protocol, which not only simplifies fabrication but also strengthens the structural integrity of HCNM by avoiding the use of corrosive acid.

HCNM-Supported Gold Nanoparticles. The physical characteristics of suspended AuNPs and HCNM-supported AuNPs are compared in Figure 2. The suspended AuNPs showed near spherical shapes under TEM (Figure 2a). On the basis of measurements of 182 AuNPs, we estimated the nominal diameter of AuNPs to be $d = 13.3(\pm2.4)$ nm (Figure S3, Supporting Information). High resolution TEM further revealed that AuNPs were polycrystalline with multiple stacking faults (Figure 2b). The absorption spectrum of AuNPs exhibited a characteristic peak at 522 nm (Figure 2c), which was typical for gold nanoparticles with diameters ranging from 12 to 15 nm.[34] AuNPs were successfully affixed on CNTs in HCNM using polyethyleneimine as linker. SEM revealed that the distribution of AuNPs on CNTs were nearly uniform without severe agglomeration (Figure 2d). The uniform distribution of AuNPs on individual CNTs was confirmed by TEM after CNTs were removed from HCNM by sonication (Figure 2e). There was no discernible change in nanoparticle morphology or size after fixation. EDX confirmed the presence of gold on modified HCNM, together with carbon from CNTs,

iron from catalyst particles inside CNTs, and copper from the TEM grid (Figure 2f).

The quality of AuNPs attached to HCNM using LBL is comparable to the quality of cobalt nanoparticles decorated on HCNM using sputtering.[19] Compared to physical methods such as sputtering, layer-by-layer assembly is a solution-based chemical method that uses inexpensive equipment and is readily scalable for industrial applications.[35,36] The moderate processing condition used in LBL (e.g., room temperature) protects CNTs from physical damage.[37] In theory, LBL allows the fixation of any premade nanoparticles whose morphology and size can be adjusted before the fixation operation.[38,39] Separating steps of nanoparticle preparation and fixation can lead to improved quality control.

Catalytic Reduction of *p*-Nitrophenol. The reduction of PNP by NaBH$_4$ is a well-studied reaction, which only occurs in the presence of catalysts such as gold nanoparticles.[40] In our experiments, the procession of the catalytic reaction was readily discerned as the yellow color of the solution faded away with time in the presence of suspended AuNPs or HCNM-supported AuNPs. As shown in Figure 3a, the absorption spectrum of PNP in NaBH$_4$ peaked at 400 nm in the presence of NaBH$_4$, due to the formation of *p*-nitrophenolate from deprotonation (pK_a = 7.2).[41] AuNPs can facilitate electron transfer from from BH$_4^-$ to *p*-nitrophenolate and thus lower the barrier of activation energy for reducing PNP to *p*-aminophenol. As shown in Figure 3a, *p*-aminophenol absorbed minimal light from 325 to 600 nm.[42,43] A comparison of the absorption spectra between PNP and *p*-aminophenol suggested that a simple but effective method to quantify the kinetics of the reaction was measuring the absorbance at 400 nm (see Figure S4, Supporting Information, for calibration).

We first compared performances of suspended AuNPs and HCNM-supported AuNPs in batch experiments. As shown in Figure 3b, changes of PNP concentration, C, for both catalysts conformed to the pseudo first-order rate law

$$\ln \frac{C}{C_0} = -k_1 t \tag{1}$$

where C_0 is initial concentration, t is reaction time in seconds, and k_1 is the rate constant. Reaction kinetics was independent of $NaBH_4$ concentration because $NaBH_4$ was in excess ($[NaBH_4]:[PNP] \geq 250$). The reaction kinetics was also independent of initial PNP concentration, as evident from the overlaying of data points obtained with $C_0 = 0.05$, 0.1, and 0.2 mM. Least-square regressions yielded $k_1(AuNPs) = 6.3(\pm0.1) \times 10^{-3}$ s^{-1} ($R^2 = 0.99$) and $k_1(HCNM-AuNPs) = 13.3(\pm1.1) \times 10^{-3}$ s^{-1} ($R^2 = 0.98$). The first-order rate constant was normalized to the ratio of solution volume to AuNPs' surface area

$$k = k_1 \frac{\rho d V}{6m} \tag{2}$$

where m is gold mass (7.4 μg for AuNPs and 20 μg for HCNM-AuNPs), ρ is gold density (19.6 g cm^{-3}),[44] V is solution volume (3 mL), and d is the AuNP diameter (13.3($\pm$2.4) nm; cf. Figure S3, Supporting Information). According to eq 2, we calculated $k(AuNPs) = 111(\pm2)$ μm s^{-1} and $k(HCNM-AuNPs) = 87(\pm7)$ μm s^{-1}. The ratio of $k(AuNPs)$ to $k(HCNM-AuNPs)$ was 78%, indicating that most of AuNP surfaces remained accessible to reactants after attaching to CNTs. The slight decrease of reactivity was likely due to the blockage of part of the AuNP surface at the AuNP–CNT juncture, as depicted in Figure 3c.

After confirming that AuNPs attached to HCNM maintained most of their catalytic capability, we performed flow-through experiments to assess the potential of AuNPs-decorated HCNM for continuous operation, as illustrated in Figure 3d. The reduction of PNP decreased with increasing flow rate according to the first-order rate law, as shown in Figure 3e

$$\ln \frac{C}{C_0} = -\frac{k^*}{f} \frac{\rho d A}{6m} \tag{3}$$

where f is water flux in cm s^{-1}, k^* is the rate constant, and A is the HCNM surface area. The term $\rho dA/(6m)$ represents the ratio of total AuNP surface area to membrane surface area, which was 18.4 in our experiments ($m = 80$ μg and $A = 1$ cm^2). Least square regression gave $k^*(HCNM-AuNPs) = 62(\pm4)$ μm s^{-1}. The rate constant measured for the flow-through configuration was 71% of the rate constant under the batch configuration: $k^*/k(HCNM-AuNPs) = 0.71$. At $f \leq 40$ cm min^{-1}, water flowed through the HCNM pores (i.e., $l = 10-38$ μm) had a low Reynolds number: $Re \leq flv^{-1}\phi^{-1} = 3.8$, where $v = 0.01$ cm^2 s^{-1} was the kinematic viscosity of water,[44] and $\phi \approx 0.36$ was the porosity of SSM. The low Reynolds number would have suggested a laminar flow with minimal mixing and thus slow kinetics for surface-catalyzed PNP reduction. On the contrary, the fast kinetics that we measured suggested that mixing inside HCNM pores (cross-section area ≥ 100 μm^2) was enhanced by the hierarchical structure of CNT arrays. This may be similar to the chaotic mixing effect in microfluidic channels coated with CNT arrays.[45] We hypothesize that in the pressured flow, CNTs inside the mesh openings can move vigorously like trees in a tornado, which creates the condition for chaotic mixing.

In Table 1, we compare the first-order rate constants of PNP reduction under the catalysis of AuNPs obtained in this study with the data in the literature. For suspended AuNPs, our result

Table 1. First-Order Rate Constants of p-Nitrophenol Reduction Catalyzed by Suspended and Supported Gold Nanoparticles

catalyst	AuNP size (nm)	rate constant[a] (μm s^{-1})	reference
suspended in batch reactors			
	12	140	16
	13.3($\pm$2.4)	111($\pm$2)	this study
	200($\pm$44)	7.18	51
supported in flow-through reactors			
AAO membrane	12	180	16
HCNM	13.3($\pm$2.4)	62($\pm$4)	this study

[a]The rate constants are normalized to the surface area of nanoparticles.

of $k = 111(\pm2)$ μm s^{-1} measured in well-mixed batch reactors is comparable to the rate constant obtained by Dotzauer and colleagues using AuNPs with similar sizes.[16] Dotzauer and colleagues attached their AuNPs on the AAO membrane and obtained a rate constant of 180 μm s^{-1}, which is approximately 3 times our result of $k^* = 62(\pm4)$ μm s^{-1} measured for HCNM-supported AuNPs in the flow-through reactor. We suspect that the high rate constant of AAO-supported AuNPs may be attributable to the AAO membrane's small pores, which are only 200 nm in diameter. In comparison, the openings in HCNM are at least 50 times greater. Smaller pores require a shorter length for mixing by diffusion, which is proportional to the cross-section area of the pores.[46] The pressure required to push water through the pores is, however, inversely proportional to the cross-section area of the pores,[47] which implies that the AAO membrane may require much higher pressure to operate than HCNM. As the reduction of energy use becomes increasingly important for achieving sustainability, HCNM is attractive as nanoparticle support for its balanced performances in treatment efficiency and energy use.

In conclusion, we have fabricated hierarchical carbon nanotube membranes and demonstrated that AuNPs attached to HCNM retain most of their catalytic capability. Gold nanoparticles supported by HCNM do not agglomerate or require post-treatment separation. AuNP-decorated HCNM also promotes mixing that is particularly beneficial for surface-catalyzed degradation of dissolved pollutants such as PNP. Although the AuNPs-decorated HCNM used in this study is only centimeters in size, HCNM of meters in size can be produced using moving substrate systems.[48,49] Our results suggest that AuNPs-decorated HCNM is a promising material and should be further developed for catalytic degradation of recalcitrant contaminants in water.[50]

■ ASSOCIATED CONTENT

Ⓢ Supporting Information

Figure S1: XRD pattern of stainless steel mesh. Figure S2: Schematic diagram and laboratory setup of CVD. Figure S3: Size distribution of gold nanoparticles. Figure S4: Calibration of PNP concentration measurement. This material is available free of charge via the Internet at http://pubs.acs.org.

■ AUTHOR INFORMATION

Corresponding Author

*E-mail: chongzheng.na@gmail.com.

Notes

The authors declare no competing financial interest.

■ REFERENCES

(1) Pradeep, T.; Anshup. Noble metal nanoparticles for water purification: A critical review. *Thin Solid Films* **2009**, *517*, 6441−6478.

(2) Stankus, D. P.; Lohse, S. E.; Hutchison, J. E.; Nason, J. A. Interactions between natural organic matter and gold nanoparticles stabilized with different organic capping agents. *Environ. Sci. Technol.* **2011**, *45*, 3238−3244.

(3) Alvarez, P. J. J.; Colvin, V.; Lead, J.; Stone, V. Research priorities to advance eco-responsible nanotechnology. *ACS Nano* **2009**, *3*, 1616−1619.

(4) Kuroda, K.; Ishida, T.; Haruta, M. Reduction of 4-nitrophenol to 4-aminophenol over Au nanoparticles deposited on PMMA. *J. Mol. Catal A: Chem.* **2009**, *298*, 7−11.

(5) Qiu, L.; Peng, Y.; Liu, B.; Lin, B.; Peng, Y.; Malik, M. J.; Yan, F. Polypyrrole nanotube-supported gold nanoparticles: An efficient electrocatalyst for oxygen reduction and catalytic reduction of 4-nitrophenol. *Appl. Catal., A* **2012**, *413−414*, 230−237.

(6) Han, J.; Li, L.; Guo, R. Novel approach to controllable synthesis of gold nanoparticles supported on polyaniline nanofibers. *Macromolecules* **2010**, *43*, 10636−10644.

(7) Zhang, J.; Chen, G.; Chaker, M.; Rosei, F.; Ma, D. Gold nanoparticle decorated ceria nanotubes with significantly high catalytic activity for the reduction of nitrophenol and mechanism study. *Appl. Catal., B* **2013**, *132−133*, 107−115.

(8) Fazzini, S.; Nanni, D.; Ballarin, B.; Cassani, M. C.; Giorgetti, M.; Maccato, C.; Trapananti, A.; Aquilanti, G.; Ahmed, S. I. Straightforward synthesis of gold nanoparticles supported on commercial silica−polyethyleneimine beads. *J. Phys. Chem. C* **2012**, *116*, 25434−25443.

(9) Zhu, Y.; Shen, J.; Zhou, K.; Chen, C.; Yang, X.; Li, C. Multifunctional magnetic composite microspheres with in situ growth Au nanoparticles: A highly efficient catalyst system. *J. Phys. Chem. C* **2010**, *115*, 1614−1619.

(10) Marcelo, G.; Muñoz-Bonilla, A.; Fernández-García, M. Magnetite−polypeptide hybrid materials decorated with gold nanoparticles: Study of their catalytic activity in 4-nitrophenol reduction. *J. Phys. Chem. C* **2012**, *116*, 24717−24725.

(11) Xuan, S.; Wang, Y.-X. J.; Yu, J. C.; Leung, K. C.-F. Preparation, characterization, and catalytic activity of core/shell Fe₃O₄@polyaniline@Au nanocomposites. *Langmuir* **2009**, *25*, 11835−11843.

(12) Lin, F.-h.; Doong, R.-a. Bifunctional Au−Fe₃O₄ heterostructures for magnetically recyclable catalysis of nitrophenol reduction. *J. Phys. Chem. C* **2011**, *115*, 6591−6598.

(13) Ge, J.; Hu, Y.; Biasini, M.; Beyermann, W. P.; Yin, Y. Superparamagnetic magnetite colloidal nanocrystal clusters. *Angew. Chem., Int. Ed.* **2007**, *46*, 4342−4345.

(14) Macanás, J.; Ouyang, L.; Bruening, M. L.; Muñoz, M.; Remigy, J. C.; Lahitte, J. F. Development of polymeric hollow fiber membranes containing catalytic metal nanoparticles. *Catal. Today* **2010**, *156*, 181−186.

(15) Ouyang, L.; Dotzauer, D. M.; Hogg, S. R.; Macanás, J.; Lahitte, J.-F.; Bruening, M. L. Catalytic hollow fiber membranes prepared using layer-by-layer adsorption of polyelectrolytes and metal nanoparticles. *Catal. Today* **2010**, *156*, 100−106.

(16) Dotzauer, D. M.; Dai, J.; Sun, L.; Bruening, M. L. Catalytic membranes prepared using layer-by-layer adsorption of polyelectrolyte/metal nanoparticle films in porous supports. *Nano Lett.* **2006**, *6*, 2268−2272.

(17) Lakes, R. Materials with structural hierarchy. *Nature* **1993**, *361*, 511−515.

(18) Clean Water Act Priority Pollutant List. U.S. Environmental Protection Agency, *Code of Federal Regulations*, p 40, CFR 423, Appendix A, 1982.

(19) Sano, N.; Hori, Y.; Yamamoto, S.; Tamon, H. A simple oxidation−reduction process for the activation of a stainless steel surface to synthesize multi-walled carbon nanotubes and its application to phenol degradation in water. *Carbon* **2012**, *50*, 115−122.

(20) Sano, N.; Kodama, T.; Tamon, H. Direct synthesis of carbon nanotubes on stainless steel electrode for enhanced catalyst efficiency in a glucose fuel cell. *Carbon* **2013**, *55*, 365−368.

(21) Martínez-Hansen, V.; Latorre, N.; Royo, C.; Romeo, E.; García-Bordejé, E.; Monzón, A. Development of aligned carbon nanotubes layers over stainless steel mesh monoliths. *Catal. Today* **2009**, *147*, S71−S75.

(22) Futaba, D. N.; Goto, J.; Yasuda, S.; Yamada, T.; Yumura, M.; Hata, K. General rules governing the highly efficient growth of carbon nanotubes. *Adv. Mater.* **2009**, *21*, 4811−4815.

(23) Stadermann, M.; Sherlock, S. P.; In, J.-B.; Fornasiero, F.; Park, H. G.; Artyukhin, A. B.; Wang, Y.; De Yoreo, J. J.; Grigoropoulos, C. P.; Bakajin, O.; Chernov, A. A.; Noy, A. Mechanism and kinetics of growth termination in controlled chemical vapor deposition growth of multiwall carbon nanotube arrays. *Nano Lett.* **2009**, *9*, 738−744.

(24) Frens, G. Controlled nucleation for the regulation of the particle size in monodisperse gold suspensions. *Nature Phys. Sci.* **1973**, *241*, 20−22.

(25) Dresselhaus, M. S.; Dresselhaus, G.; Saito, R.; Jorio, A. Raman spectroscopy of carbon nanotubes. *Phys. Rep.* **2005**, *409*, 47−99.

(26) Flahaut, E.; Govindaraj, A.; Peigney, A.; Laurent, C.; Rousset, A.; Rao, C. N. R. Synthesis of single-walled carbon nanotubes using binary (Fe, Co, Ni) alloy nanoparticles prepared in situ by the reduction of oxide solid solutions. *Chem. Phys. Lett.* **1999**, *300*, 236−242.

(27) Tsoufis, T.; Xidas, P.; Jankovic, L.; Gournis, D.; Saranti, A.; Bakas, T.; Karakassides, M. A. Catalytic production of carbon nanotubes over Fe−Ni bimetallic catalysts supported on MgO. *Diamond Relat. Mater.* **2007**, *16*, 155−160.

(28) Gao, L. Z.; Kiwi-Minsker, L.; Renken, A. Growth of carbon nanotubes and microfibers over stainless steel mesh by cracking of methane. *Surf. Coat. Technol.* **2008**, *202*, 3029−3042.

(29) Lee, C. H.; Johnson, N.; Drelich, J.; Yap, Y. K. The performance of superhydrophobic and superoleophilic carbon nanotube meshes in water−oil filtration. *Carbon* **2011**, *49*, 669−676.

(30) Lee, C.; Baik, S. Vertically-aligned carbon nano-tube membrane filters with superhydrophobicity and superoleophilicity. *Carbon* **2010**, *48*, 2192−2197.

(31) Zhou, Q.; Li, C.; Gu, F.; Du, H. L. Flame synthesis of carbon nanotubes with high density on stainless steel mesh. *J. Alloys Compd.* **2008**, *463*, 317−322.

(32) Zhang, Q.; Huang, J.-Q.; Zhao, M.-Q.; Qian, W.-Z.; Wang, Y.; Wei, F. Radial growth of vertically aligned carbon nanotube arrays from ethylene on ceramic spheres. *Carbon* **2008**, *46*, 1152−1158.

(33) Yamamoto, N.; John Hart, A.; Garcia, E. J.; Wicks, S. S.; Duong, H. M.; Slocum, A. H.; Wardle, B. L. High-yield growth and morphology control of aligned carbon nanotubes on ceramic fibers for multifunctional enhancement of structural composites. *Carbon* **2009**, *47*, 551−560.

(34) Jana, N. R.; Gearheart, L.; Murphy, C. J. Seeding growth for size control of 5−40 nm diameter gold nanoparticles. *Langmuir* **2001**, *17*, 6782−6786.

(35) Lvov, Y.; Decher, G.; Moehwald, H. Assembly, structural characterization, and thermal behavior of layer-by-layer deposited ultrathin films of poly(vinyl sulfate) and poly(allylamine). *Langmuir* **1993**, *9*, 481−486.

(36) Decher, G. Fuzzy nanoassemblies: Toward layered polymeric multicomposites. *Science* **1997**, *277*, 1232−1237.

(37) Dimiev, A.; Kosynkin, D. V.; Sinitskii, A.; Slesarev, A.; Sun, Z.; Tour, J. M. Layer-by-layer removal of graphene for device patterning. *Science* **2011**, *331*, 1168−1172.

(38) Cushing, B. L.; Kolesnichenko, V. L.; O'Connor, C. J. Recent advances in the liquid-phase syntheses of inorganic nanoparticles. *Chem. Rev.* **2004**, *104*, 3893−3946.

(39) Barnard, A. S. Direct comparison of kinetic and thermodynamic influences on gold nanomorphology. *Acc. Chem. Res.* **2012**, *45*, 1688−1697.

(40) Pradhan, N.; Pal, A.; Pal, T. Catalytic reduction of aromatic nitro compounds by coinage metal nanoparticles. *Langmuir* **2001**, *17*, 1800−1802.

(41) Liu, J.; Qin, G.; Raveendran, P.; Ikushima, Y. Facile "green" synthesis, characterization, and catalytic function of β-D-glucose-stabilized Au nanocrystals. *Chem.—Eur. J.* **2006**, *12*, 2131−2138.

(42) Dotzauer, D. M.; Bhattacharjee, S.; Wen, Y.; Bruening, M. L. Nanoparticle-containing membranes for the catalytic reduction of nitroaromatic compounds. *Langmuir* **2009**, *25*, 1865−1871.

(43) Ballarin, B.; Cassani, M. C.; Tonelli, D.; Boanini, E.; Albonetti, S.; Blosi, M.; Gazzano, M. Gold nanoparticle-containing membranes from in situ reduction of a Gold(III)−aminoethylimidazolium aurate salt. *J. Phys. Chem. C* **2010**, *114*, 9693−9701.

(44) Lide, D. R. *CRC Handbook of Chemistry and Physics*; CRC Press: New York, 2006.

(45) Battiato, I.; Bandaru, P. R.; Tartakovsky, D. M. Elastic response of carbon nanotube forests to aerodynamic stresses. *Phys. Rev. Lett.* **2010**, *105*, 144504.

(46) Stroock, A. D.; Dertinger, S. K. W.; Ajdari, A.; Mezic, I.; Stone, H. A.; Whitesides, G. M. Chaotic mixer for microchannels. *Science* **2002**, *295*, 647−651.

(47) Pfitzner, J. Poiseuille and his law. *Anaesthesia* **1976**, *31*, 273−275.

(48) Guzmán de Villoria, R.; et al. High-yield growth of vertically aligned carbon nanotubes on a continuously moving substrate. *Nanotechnology* **2009**, *20*, 405611.

(49) Guzmán de Villoria, R.; Hart, A. J.; Wardle, B. L. Continuous high-yield production of vertically aligned carbon nanotubes on 2D and 3D substrates. *ACS Nano* **2011**, *5*, 4850−4857.

(50) Pirkanniemi, K.; Sillanpaa, M. Heterogeneous water phase catalysis as an environmental application: A review. *Chemosphere* **2002**, *48*, 1047−1060.